Journal of Magnetic Resonance 384 (2026) 108021

Contents lists available at ScienceDirect

Journal of Magnetic Resonance

journal homepage: www.elsevier.com/locate/jmr

Heisenberg spin exchange and relaxation dynamics in EPR oximetry: A photoinduced transition from non-adiabatic rapid-sweeps to the rapid-scan regime

Florian Johannsen *, Malte Drescher [1]

Department of Chemistry and Konstanz Research School Chemical Biology, University of Konstanz, Universitätsstraße 10, Konstanz, 78464, Germany

ARTICLE INFO

Keywords:
Rapid-scan EPR
EPR oximetry
Nitroxide spin probes
Lithium phthalocyanine
Heisenberg spin exchange
Spin relaxation
Photopolymerization

ABSTRACT

Rapid-scan electron paramagnetic resonance spectroscopy (RS EPR) has emerged as a powerful tool to monitor light-induced processes accompanied by changes of the EPR lineshape and is frequently used for measuring local oxygen concentrations. Here we use LiPc (lithium phthalocyanine) and CTPO (3-Carbamoyl-2,2,5,5-tetramethyl-3-pyrrolin-1-oxyl) as spin probes and demonstrate control over the oxygen partial pressure through a photochemical reaction. The resulting changes in pO_2 manifest as characteristic distortions of the EPR lineshape and reveal how Heisenberg spin exchange influences relaxation dynamics. As a proof-of-concept, we investigate photopolymerization at reduced oxygen levels. These results highlight the potential of RS for studying oxidation processes in biochemical systems.

1. Introduction

Oxygen is one of the key players in many physiological processes and viewed as an important variable for clinical applications such as radiotherapy or hemodialysis. Oxygen influences wound healing, blood flow, drug delivery and is one of the primary reactants in metabolism and cell growth [1]. Beyond biological systems, oxygen also plays a crucial role in photopolymerization [2]. Rapid-scan electron paramagnetic resonance spectroscopy (RS EPR) has previously been applied to image oxygen consumption during photopolymerization and post-curing highlighting the capabilities of EPR to improve the quality and resolution of 3D prints by optimizing light exposure [3,4].

Comprehensive studies, either biochemical or related to material science, require not only monitoring of oxygen but also to precisely control local O_2 levels. Here, we use RS EPR and employ a photochemical reaction for regulating the oxygen partial pressure in solution. The goal of this article is to explore how molecular oxygen influences spin relaxation through Heisenberg spin exchange. This allows monitoring of the transition into the rapid-scan regime under carefully controlled experimental conditions. As a proof-of-concept, we investigate photopolymerization at reduced oxygen levels.

2. Rapid-scan EPR oximetry

EPR oximetry is a sophisticated, highly versatile technique for measuring oxygen concentrations in biological and chemical systems using electron paramagnetic resonance spectroscopy. In this method, paramagnetic molecules are employed whose spectral characteristics change in response to variations in oxygen partial pressure. Historically, oxygen-sensitive nitroxides were utilized first as they exhibit oxygen-dependent line broadening. Nitroxide radicals are soluble, can be used in extra- and intracellular compartments and are capable to penetrate the blood–brain barrier [5]. A major disadvantage of nitroxide probes is metabolic conversion to EPR-silent hydroxylamines leading to a progressive loss in signal intensity.

Particulate materials such as lithium phthalocyanine (LiPc) are less susceptible to bioreduction and have emerged as the probe of choice due to their superior sensitivity, spectral shape and biocompatibility. LiPc features a narrow single line EPR spectrum whose linewidth increases linearly (5.1 mG/mmHg) over a wide range of oxygen levels and has successfully been used for long-term in vivo studies [6].

The functionality of LiPc as a probe for local oxygen concentrations, as with nitroxides, is based on the Heisenberg spin exchange (HSE). HSE is a short-range interaction between paramagnetic species which comes into play when the wavefunctions of the unpaired electrons overlap.

* Corresponding author.
E-mail addresses: florian.johannsen@uni-konstanz.de (F. Johannsen), malte.drescher@uni-konstanz.de (M. Drescher).
[1] Current address: RPTU University Kaiserslautern-Landau, Kaiserslautern, 67633, Germany.

https://doi.org/10.1016/j.jmr.2026.108021
Received 10 October 2025; Received in revised form 20 January 2026; Accepted 25 January 2026
Available online 27 January 2026
1090-7807/© 2026 The Author(s). Published by Elsevier Inc. This is an open access article under the CC BY license (http://creativecommons.org/licenses/by/4.0/).

Konstanzer Online-Publikations-System (KOPS)
URL: http://nbn-resolving.de/urn:nbn:de:bsz:352-2-9ypiexm3j9t99

Under these conditions, there is a certain probability of exchanging their spin coordinates. This shortens the lifetime for the involved spin states, decreases spin relaxation times and leads to line broadening of the EPR spectrum [7]. The rate of spin exchange is proportional to the concentration of paramagnetic species. Molecular oxygen is paramagnetic in its electronic ground state $^3O_2$ and, mainly through collisions increases the relaxation rate via HSE. Since spin exchange is a purely physical interaction, no oxygen is consumed. EPR oximetry is non-invasive and perfectly suited for investigations of biochemical systems.

LiPc (Fig. 2 I) is particularly interesting to study with RS-EPR. RS finds itself between pulsed and continuous wave (CW) EPR in the sense that microwave power and frequency are set to constant values. CW spectroscopy uses phase sensitive detection and magnetic fields that slowly traverse the resonance to produce the familiar first derivative display of the absorption signal. RS experiments are conducted with the main magnetic field centered at resonance but modulated to pass through the entire spectrum thousands of times per second. In this way, similar to pulsed EPR, the resonance condition is only satisfied for a short period of time.

Fig. 1a illustrates the change in lineshape of a single spin packet with increasing spin relaxation time, a scenario expected for LiPc during deoxygenation. A pure Lorentzian is observed if the resonance is traversed slow relative to relaxation times, i.e. the spin system remains in thermal equilibrium during the time on resonance. A situation referred to as non-adiabatic rapid sweeps (NARS). Scanning through the spectrum with scan rates that satisfy the condition

$$\left|\frac{B_1}{\mathrm{d}B_z/\mathrm{d}t}\right| \ll \sqrt{T_1 T_2} \tag{1}$$

causes oscillations on the trailing edge of the signal [8]. These so-called passage effects appear in the rapid-scan regime and, for a single resonance line, look very similar to a free induction decay.

Another linewidth dependent change associated with Heisenberg spin exchange in response to oxygen can be observed for the CTPO nitroxide radical (Fig. 2 II). CTPO, in oxygen-free conditions, exhibits a well-resolved multiline spectrum characterized by a distinct proton superhyperfine structure [9]. If oxygen is introduced into the system, spectral resolution decreases and broadening results in a typical three-line nitroxide spectrum. Determination of the oxygen concentration is achieved by detection of only one of the three lines. Usually that of the center field peak (Fig. 1b). If inhomogeneous broadening mechanisms do not cause transient oscillations to interfere destructively, passage effects may be present.

In this work, we use methylene blue (MB, Fig. 2 III), a common photosensitizer, to generate singlet oxygen $^1O_2$ from paramagnetic triplet oxygen which binds to anthracene (Fig. 2 IV) to remove oxygen from aqueous solutions [10,11]. The decrease in pO_2 leads to reduced HSE, narrower EPR linewidths, longer spin relaxation times and ultimately, the appearance of passage effects in the rapid-scan regime.

For demonstration purposes, we deoxygenate a TMPTA (Fig. 2 V) monomer solution and initiate polymerization by activation of a triazine-based photoinitiator (Fig. 2 VI). This process creates stable radicals that are trapped within the cross-linked polymer network leading to an EPR signal that reflects molecular mobility and monomer conversion after vitrification.

3. Experimental section

3.1. Spectroscopy and parameter selection

The pO_2 vs. linewidth calibration for LiPc was performed using a 25 mT CW spectrometer/imager operating at 684 MHz frequency, developed by O2M Technologies. Each measurement was performed with a modulation frequency of 15.26 kHz. Modulation amplitude and microwave power were adjusted according to the signal intensity and linewidth at each partial oxygen pressure. Nine data points from 0 to 160 mmHg were acquired and each reported value is the average across ten measurements.

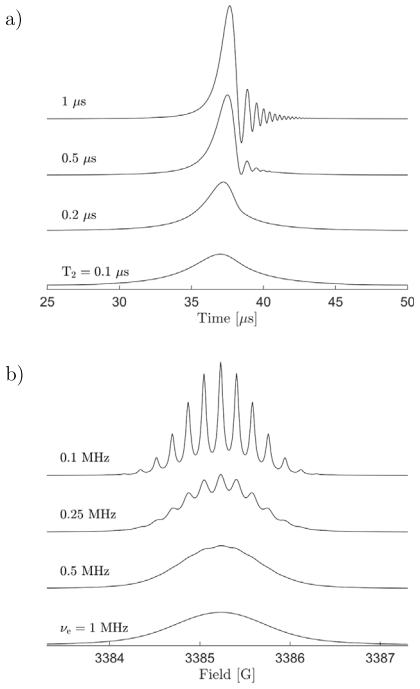

Fig. 1. Different manifestations of Heisenberg spin exchange on the EPR lineshape of two oxygen-sensitive spin probes. (a) LiPc: Simulated rapid-scan signal obtained by numerical integration of the modified Bloch equations. Transient oscillations on the trailing edge become more pronounced with increasing spin-spin relaxation time T_2. (b) CTPO: Simulation of the centerfield peak in the isotropic fast-motional regime. The nitroxide exhibits a thirteen-line pattern in the absence of oxygen. Heisenberg spin exchange results in broadening of the spectrum and a less evident superhyperfine structure. Time and magnetic field axes can be interconverted using known expressions for the rapidly changing modulation field. Exchange frequencies were calculated from the linewidth of the spectrum.

Rapid-scan experiments were conducted with the Bruker RS accessory, installed on an Elexsys spectrometer at X-Band. Microwave powers were chosen to remain below signal saturation and scan rates were selected to avoid substantial distortions by the modulation field, while operating close to the rapid-scan regime before initiating photochemical reactions.

Spectra of LiPc were recorded by lowering the resonator Q-factor to accurately preserve high frequency components. Time-resolved experiments were performed with a 50 G sinusoidal scan, a scan frequency of 20 kHz and 2 s data acquisition times, collected continuously over a five minute period. Irradiation of MB is carried out with a diode pumped Nd:YAG laser (EKSPLA) operating at a fixed repetition rate of 50 Hz, a pulse length of 4 ns, and unless otherwise stated, a wavelength of 660 nm. Samples were irradiated after 10 s of measuring time with the optical fiber directly coupled into the resonator from above. Spectra of CTPO were recorded before and after irradiation with measurement times of 2 min each. A 10 G wide scan was sufficient for covering the central resonance line. Polymer samples required a 200 G sinusoidal scan with Q-factors that needed be reduced only if LiPc was included to measure oxygen concentrations. Dynamic light scattering (on a Malvern Zetasizer Nano) was performed for verification of higher monomer conversion at lower pO_2 levels.

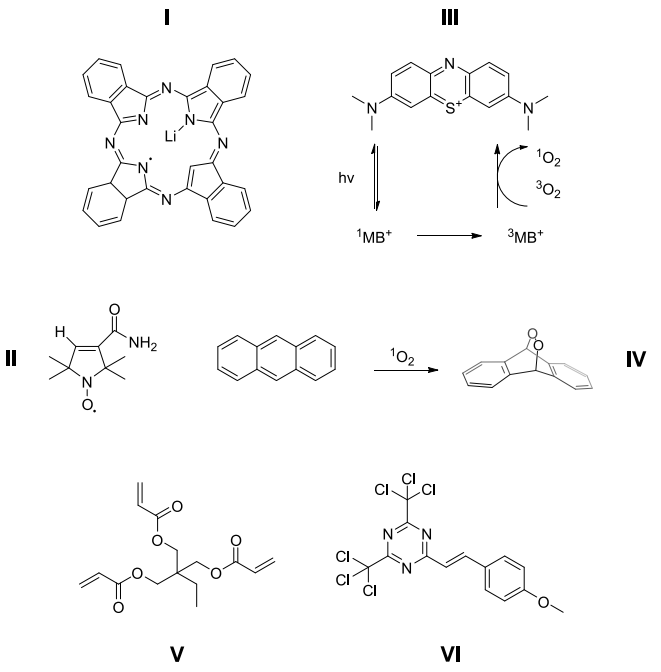

Fig. 2. (I) LiPc (Lithium phthalocyanine). (II) CTPO (3-Carbamoyl-2,2,5,5-tetramethyl-3-pyrrolin-1-oxyl). (III) Generation of singlet oxygen $^1O_2$ through energy transfer between paramagnetic triplet oxygen $^3O_2$ and photoexcited methylene blue (MB). (IV) Trapping of $^1O_2$ with anthracene. (V) TMPTA (Trimethylolpropane triacrylate). (VI) Photoinitiator (2-(4-Methoxystyryl)-4,6-bis(trichloromethyl)-1,3,5-triazine).

3.2. Samples

Oxygen sensitive LiPc crystals were synthesized at O2M using an electrochemical synthesis method that has been reported before [12]. Solutions for calibration were prepared placing 10 mg of grinded LiPc into a 10×75 mm (DxL) borosilicate glass tube and contained 450 µL of deionized H_2O, 500 µL of anthracene (10 mM), and 50 µL of methylene blue (10 mM). To obtain the desired pO_2, a gas mixture of O_2 and N_2 was bubbled through the solution for approximately 1.5 h.
For RS measurements, 0.2 mg of LiPc were placed in an Eppendorf tube and mixed with 9 µL MilliQ-water, 10 µL anthracene (10 mM), and 1 µL of methylene blue in concentrations varying from 0 to 10 mM. The solution was loaded into a 50 µL Hirschmann capillary and placed inside the resonator in a wider guide tube. The CTPO sample was prepared with 1 µL of a 5 mM stock solution replacing 1 µL of MilliQ-water.
TMPTA samples contained 20 µL of the monomer, 2 µL anthracene (50 mM), 2 µL of the photoinitiator (10 mM), 1 µL methylene blue (1 mM) and, when oxygen measurements were intended 0.2 mg LiPc. Dynamic light scattering was carried out after diluting irradiated samples to a final TMPTA concentration of 2 mg/mL in methanol. Photoinitiator, anthracene and methylene blue were dissolved in DMSO.

3.3. Data processing and analysis

Post-processing of RS signals is done using a locally-written software in Matlab and is based on previously published algorithms. Briefly, quadrature detected RS spectra are phase-corrected by multiplication with a complex exponential and divided into separate parts for the up- and downfield scan. The sinusoidal background is reconstructed using non-quadratic cost-functions and subtracted from the signal [13]. The corresponding part of the spectral array that does not contain the actual EPR signal is zero-padded to correct for the non-orthogonality of the signal channels [14]. High frequency noise is removed using a 5th-order Butterworth filter with a cutoff frequency of 100 MHz. Deconvolution is applied and the equivalent slow-scan spectrum is fitted to a pair of Lorentzians [15]. This accounts for minor contributions of LiPc polymorphs which contribute to the overall EPR signal without being oxygen-sensitive [16]. A factor of $1/\sqrt{3}$ is included for pO_2 readout, i.e. comparing the full width at half maximum of the absorption line with the peak-to-peak CW EPR linewidth obtained for calibration.
A sample data set of LiPc illustrating the data processing procedure is shown in Fig. 3.

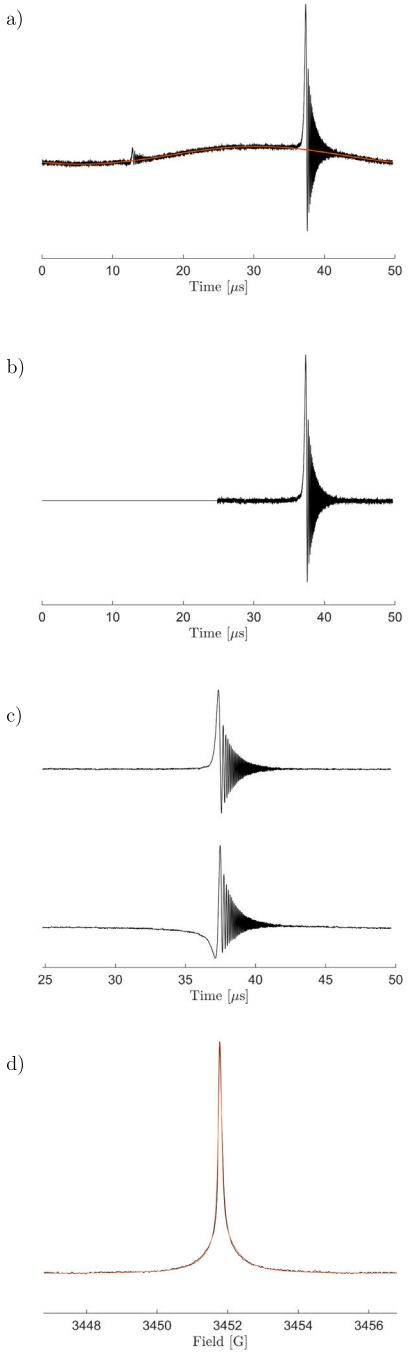

Fig. 3. Data processing. (a) Phase corrected rapid-scan signal and reconstruction of the background (red) using non-quadratic cost functions. (b) Background corrected rapid-scan signal. Zeroing of the spectral array belonging to the first half cycle corrects for the non-orthogonality of the signal channels. (c) Absorption and dispersion signal used for reconstruction of the undistorted rapid-scan signal. A 5th-order Butterworth filter with a cutoff frequency of 100 MHz is used to suppress high frequency noise. (d) Deconvolved rapid-scan spectrum and Lorentzian fit (red).

4. Results and discussion

4.1. Spectra of LiPc

Samples containing LiPc were irradiated at 660 nm and the decrease in pO_2 was monitored with 2 s time resolution (Fig. 4). Before switching on the laser, the lineshape is essentially Lorentzian, indicating a high rate of spin exchange with molecular oxygen.

Upon irradiation, MB converts paramagnetic triplet oxygen into singlet oxygen which is removed by reaction with anthracene. This process is accompanied by the appearance of distinct oscillations on the trailing edge of the signal. The progressive change of the EPR lineshape indicates continuous O_2 consumption and a transition into the rapid-scan regime. Spectra obtained by deconvolution exhibit a time-dependent decrease in linewidth/ pO_2.

Alternatively, rapid-scan signals can be simulated by numerical integration of the modified Bloch equations [17]. This allows T_2 to be extracted from experimental data and used for linewidth determination. In our simulations, we used the Levenberg–Marquardt algorithm employing the least possible number of fitting parameters: a scaling factor, the microwave phase, T_2, and a small offset from the resonance field. Linewidths derived from T_2 values are consistent with those obtained from deconvolution, albeit greater variability. This demonstrates the strong relation between line broadening and spin-relaxation dynamics. Samples containing different amounts of MB are identical in pO_2 before irradiation but differ in their oxygen concentration afterwards. In the absence of MB, no oxygen is consumed leaving the EPR linewidth unchanged. High concentrations, impact energy transfer to ground state oxygen by formation of dimers leading to only a moderate decrease in pO_2 [18].

Note that pO_2 values were determined using the calibration shown in Fig. 4(c). Differences in microwave frequency, instrumental factors, magnetic field inhomogeneities, and possibly a better resolved g-anisotropy at X-Band can lead to increased linewidths. Determined oxygen concentrations are slightly higher than the nominal 160 mmHg for a fully oxygenated solution at ambient pressure.

A Matlab script for fitting experimental data using the modified Bloch equations is provided in the supporting information of this article.

4.2. Spectra of CTPO

Spectra of CTPO were acquired before and after 5 min of irradiation. In air-saturated solution, the superhyperfine splitting is barely visible. Differences in the spectra are more pronounced in the first-derivative display obtained using pseudomodulation (Fig. 5).

The reduced spectral resolution before irradiation is a direct consequence of HSE which is observed when the exchange frequency ω_{ex} is close to the difference of the EPR frequency caused by the proton hyperfine coupling, i.e. $\omega_{ex} \approx \gamma a_H$ [7]. To validate this criterion, experimental data were fitted taking into account twelve equivalent methyl protons, a single ring proton and contributions of the ^{13}C isotope. Exchange frequencies were estimated from the linewidth of the spectra

$$\omega_{ex} \approx \frac{\sqrt{3}}{2}\gamma \Delta B_{pp}(pO_2) \tag{2}$$

using the gyromagnetic ratio to convert between magnetic field units and angular frequency [19,20]. Simulations incorporated the same modulation amplitude as in the calculation of pseudomodulated signals. In oxygen-rich environment, molecular oxygen induces significant broadening, causing the superhyperfine structure to appear largely unresolved. This observation, confirmed by our simulations, is consistent with exchange frequencies exceeding the hyperfine coupling $\omega_{ex} > \gamma a_H$. As oxygen is removed, spectral resolution increases, the proton hyperfine lines become more pronounced and $\omega_{ex} < \gamma a_H$ holds true.

A Matlab script for pseudomodulation and a spectrum showing passage effects can be found in the supporting information.

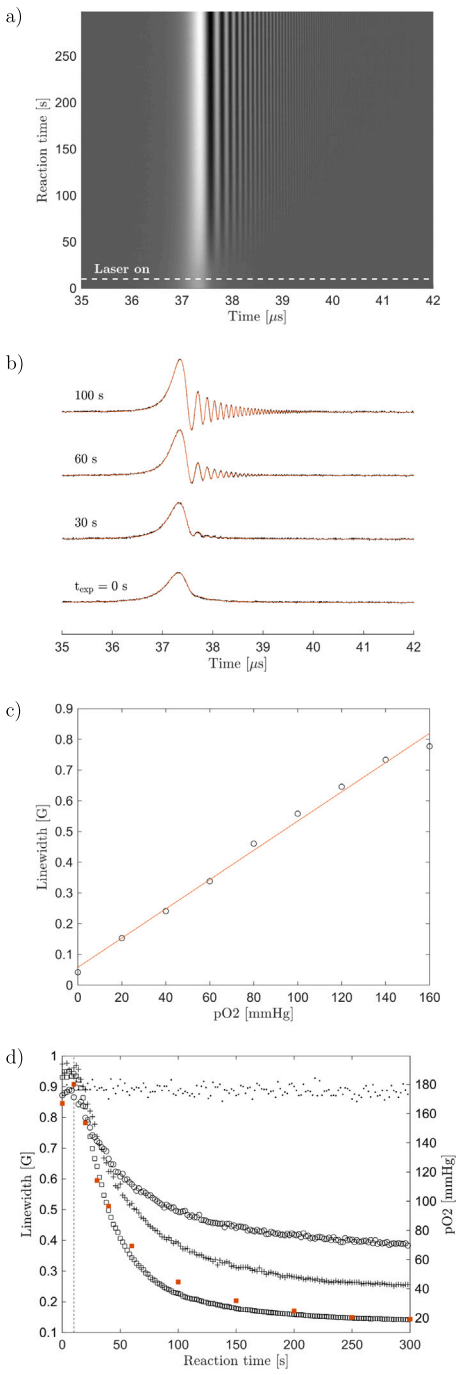

Fig. 4. Time resolved RS experiment of LiPc (X-Band). (a) 2D-spectrum. The reaction time is displayed on the vertical axis. Signal intensities are color coded. Photoexcitation is followed by a transition into the RS regime. (b) Slices at different instances. Fitting by numerical integration of the modified Bloch-equations (red). (c) Calibration: Linewidth of LiPc vs. known pO_2 values measured on a CW radio-frequency imager (O2M Technologies). Linear regression (red). (d) Variations in sample composition and laser emission enable the partial pressure to be precisely controlled. Methylene blue 0 μM (dots), 50 μM (squares), 500 μM (plus), 250 μM at 600 nm (circles). Linewidth derived from T_2, obtained by fitting experimental data using the modified Bloch-equations (red squares). Note that operation at different microwave frequencies can affect absolute linewidth determination. Conversion to pO_2 values is shown for reference only.

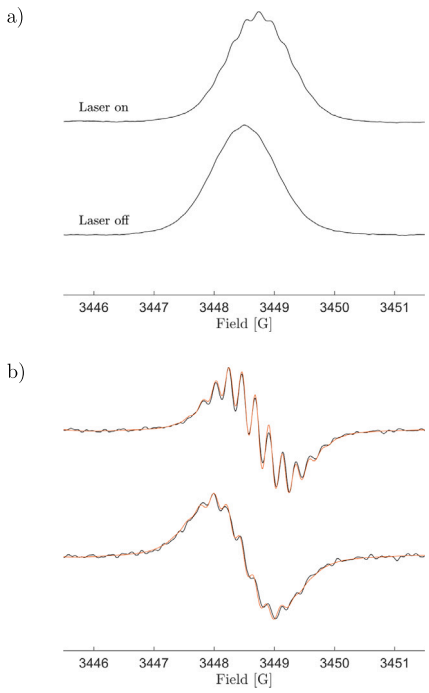

Fig. 5. Rapid-scan experiment of CTPO in solution. A sinusoidal scan with 10 G scanwidth and a modulation frequency of 20 kHz is used for detection of the centerfield peak. The microwave power is set to 2 mW. Data acquisition times were 120 s. Samples were irradiated for 5 min (660 nm, 4 mJ per pulse with a repetition rate of 50 Hz). (a) Deconvolved RS absorption signal before and after irradiation. (b) Pseudomodulated spectra and simulation (red).

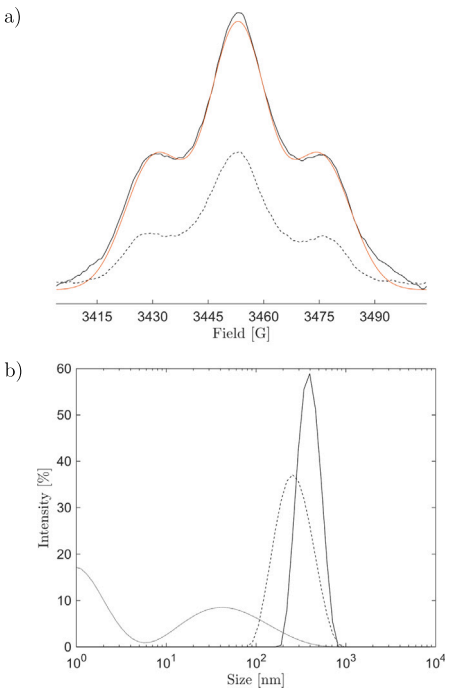

Fig. 6. EPR and DLS measurements of TMPTA. (a) RS EPR absorption line obtained after deoxygenation followed by activation of the photoinitiator (solid). Fit of the spectrum according to the mid-chain radical model (red). Spectrum of the TMPTA polymer without prior irradiation of MB (dashed). (b) Dynamic light scattering (line styles are the same as in the EPR spectra). Non-irradiated samples are highly polydisperse (dotted).

4.3. Spectra of TMPTA

TMPTA is a trifunctional acrylate that forms a highly branched network with stable radicals produced via inter- and intramolecular hydrogen abstraction (backbiting) [21,22]. This enables direct detection with EPR and insight into polymerization at reduced oxygen levels. Thus spectra of TMPTA were recorded either with or without prior irradiation of MB (Fig. 6a). Spin concentrations, calculated from the integral of the absorption line, are found to be approximately twice as high when polymerization was initiated under hypoxic conditions.
This observation is consistent with the well-known oxygen inhibition effect. Lower oxygen levels result in more efficient chain growth, enhanced backbiting, an increased number of mid-chain radicals and a larger EPR signal amplitude. Measurements with LiPc showed a decrease in the oxygen partial pressure of approximately 50 mmHg after irradiation of MB. DLS provides complementary evidence for enhanced polymer growth. Specifically, polymers formed in deoxygenated solutions exhibit a hydrodynamic radius larger by 130 nm (Fig. 6b).

5. Conclusion & outlook

In this study, we have demonstrated control over the oxygen partial pressure employing a photochemical reaction. This allowed monitoring of the transition into the rapid-scan regime and illustrates how Heisenberg spin exchange influences relaxation dynamics. The here described approach for degassing liquid solution samples offers an alternative to traditional techniques for oxygen removal such as the freeze-pump-thaw technique that is frequently used for acquisition of high-resolution spectra that would otherwise be broadened under normal atmospheric pressure. The ability to regulate local oxygen concentrations during time-resolved in situ EPR offers great potential for studying a variety of biochemical processes under hypoxic conditions. Examples include free radical polymerization as well as in vitro studies of wound healing. Methylene blue as an efficient singlet oxygen generator can also be used for oxidation of intrinsically disordered proteins which affects their aggregation behavior. Such studies, when combined with site-directed spin labeling, could provide valuable insights into misfolding and conformational rearrangements of peptides such as Alzheimer's amyloid-beta.
This work and the proposed future directions highlight the utility of rapid-scan EPR as a powerful tool for investigations of light-induced oxidation processes accompanied by changes of the EPR lineshape.

CRediT authorship contribution statement

Florian Johannsen: Writing – original draft, Visualization, Formal analysis, Conceptualization. **Malte Drescher:** Writing – review & editing.

Funding

This work received funding from the European Research Council (ERC) under the European Union's Horizon 2020 research and innovation programme (Grant Agreement number: 772027-SPICEERC-2017-COG).

Declaration of competing interest

The authors declare no conflict of interest.

Acknowledgments

We gratefully acknowledge Mrignayani Kotecha (O2M Technologies, Oxygen Measurement Core, Chicago USA) for providing LiPc and performing the calibration.

Appendix A. Supplementary data

Supplementary material related to this article can be found online at https://doi.org/10.1016/j.jmr.2026.108021.

Data availability

Data will be made available on request.

References

[1] E. BEŠIĆ, Z. Rajić, D. Šakić, Advancements in electron paramagnetic resonance (EPR) spectroscopy: A comprehensive tool for pharmaceutical research, Acta Pharm. 74 (4 (Special issue)) (2024) 551–594.

[2] A.K. O'Brien, C.N. Bowman, Impact of oxygen on photopolymerization kinetics and polymer structure, Macromolecules 39 (7) (2006) 2501–2506.

[3] O. Tseytlin, R. O'Connell, V. Sivashankar, A.A. Bobko, M. Tseytlin, Rapid scan EPR oxygen imaging in photoactivated resin used for stereolithographic 3D printing, 3D Print. Addit. Manuf. 8 (6) (2021) 358–365.

[4] S. Sarvari, D. McGee, R. O'Connell, O. Tseytlin, A.A. Bobko, M. Tseytlin, Electron spin resonance probe incorporation into bioinks permits longitudinal oxygen imaging of bioprinted constructs, Mol. Imaging Biol. 26 (3) (2024) 511–524.

[5] D. Goldfarb, S. Stoll, EPR Spectroscopy: Fundamentals and Methods, John Wiley & Sons, 2018.

[6] J.F. Dunn, H.M. Swartz, In vivo electron paramagnetic resonance oximetry with particulate materials, Methods 30 (2) (2003) 159–166.

[7] V.V. Khramtsov, A.A. Bobko, M. Tseytlin, B. Driesschaert, Exchange phenomena in the electron paramagnetic resonance spectra of the nitroxyl and trityl radicals: multifunctional spectroscopy and imaging of local chemical microenvironment, Anal. Chem. 89 (9) (2017) 4758–4771.

[8] M. Weger, Passage effects in paramagnetic resonance experiments, Bell Syst. Tech. J. 39 (4) (1960) 1013–1112.

[9] Y.T. Zhou, J.J. Yin, Y.M. Lo, Application of ESR spin label oximetry in food science, Magn. Reson. Chem. 49 (2011) S105–S112.

[10] J.P. Tardivo, A. Del Giglio, C.S. De Oliveira, D.S. Gabrielli, H.C. Junqueira, D.B. Tada, D. Severino, R. de Fátima Turchiello, M.S. Baptista, Methylene blue in photodynamic therapy: From basic mechanisms to clinical applications, Photodiagnosis Photodyn. Ther. 2 (3) (2005) 175–191.

[11] R. Castro-Olivares, G. Günther, A.L. Zanocco, E. Lemp, Linear free energy relationship analysis of solvent effect on singlet oxygen reactions with mono and disubstituted anthracene derivatives, J. Photochem. Photobiol. A: Chem. 207 (2–3) (2009) 160–166.

[12] G. Ilangovan, J.L. Zweier, P. Kuppusamy, Electrochemical preparation and EPR studies of lithium phthalocyanine: evaluation of the nucleation and growth mechanism and evidence for potential-dependent phase formation, J. Phys. Chem. B 104 (17) (2000) 4047–4059.

[13] F. Johannsen, M. Drescher, Background removal from rapid-scan EPR spectra of nitroxide-based spin labels by minimizing non-quadratic cost functions, J. Magn. Reson. Open 16 (2023) 100121.

[14] M. Tseitlin, D.G. Mitchell, S.S. Eaton, G.R. Eaton, Corrections for sinusoidal background and non-orthogonality of signal channels in sinusoidal rapid magnetic field scans, J. Magn. Reson. 223 (2012) 80–84.

[15] M. Tseytlin, General solution for rapid scan EPR deconvolution problem, J. Magn. Reson. 318 (2020) 106801.

[16] G. Ilangovan, J.L. Zweier, P. Kuppusamy, Mechanism of oxygen-induced EPR line broadening in lithium phthalocyanine microcrystals, J. Magn. Reson. 170 (1) (2004) 42–48.

[17] O. Laguta, A. Sojka, A. Marko, P. Neugebauer, Rapid scan ESR: A versatile tool for the spin relaxation studies at (sub) THz frequencies, Appl. Phys. Lett. 120 (12) (2022).

[18] G.A. Shahinyan, A.Y. Amirbekyan, S.A. Markarian, Photophysical properties of methylene blue in water and in aqueous solutions of dimethylsulfoxide, Spectrochim. Acta Part A: Mol. Biomol. Spectrosc. 217 (2019) 170–175.

[19] A.I. Smirnov, R. Clarkson, R. Belford, EPR linewidth (T2) method to measure oxygen permeability of phospholipid bilayers and its use to study the effect of low ethanol concentrations, J. Magn. Reson. B 111 (2) (1996) 149–157.

[20] W.K. Subczynski, J.S. Hyde, Diffusion of oxygen in water and hydrocarbons using an electron spin resonance spin-label technique, Biophys. J. 45 (4) (1984) 743–748.

[21] D. Doetschman, R. Mehlenbacher, D. Cywar, Stable free radicals produced in acrylate and methacrylate free radical polymerization: Comparative EPR studies of structure and the effects of cross-linking, Macromolecules 29 (5) (1996) 1807–1816.

[22] T. Junkers, C. Barner-Kowollik, The role of mid-chain radicals in acrylate free radical polymerization: Branching and scission, J. Polym. Sci. Part A: Polym. Chem. 46 (23) (2008) 7585–7605.